Proceedings Paper:

6th CIRP Conference on Surface Integrity

Analysis of the contact mechanics in machining using a novel high-speed tribometer

Joshua Priest[a,b]*, Hassan Ghadbeigi[b], Sabino Ayvar-Soberanis[c], Anders Liljerehn[d], Matthew Way[e]

[a] *Industrial Doctoral Centre in Machining Science, Advanced Manufacturing Research Centre with Boeing, University of Sheffield, Rotherham, S60 5TZ, UK*
[b] *The University of Sheffield, Department of Mechanical Engineering, Sir Fredrick Mappin Building, Mappin Street, S1 3JD, Sheffield, UK*
[c] *Advanced Manufacturing Research Centre with Boeing, Advanced Manufacturing Park, Catcliffe, Rotherham, S60 5TZ, UK*
[d] *Sandvik Coromant AB, Mossvägen 10, Sandviken, Sweden*
[e] *Sandvik Coromant AB , Unit 8, Morse Way, Waverley, Rotherham, S60 5BJ, UK*

* Corresponding author. Tel.: N/A; fax: N/A. *E-mail address:* j.priest@amrc.co.uk

Abstract

A new high-speed pin-on-bar type tribometer has been developed to study the variation of the friction coefficient with respect to the local thermomechanical contact conditions between the tool and the workpiece when drilling C45 steel. The forces and temperatures are measured over a range of pin indent depths and sliding velocities in open and closed loop tribo-systems. The tribometer's ability to recreate the thermomechanical contact conditions in drilling is demonstrated and the induced surface modification in the workpiece by the tribology testing is studied.

Keywords: contact; friction; drilling; tribometer

1. Introduction

An accurate and realistic coefficient of friction (COF) between the tool-chip and the tool-workpiece is critical in machining simulations as this impacts the predicted forces, chip geometry, machined surface integrity, and the rate of tool wear [1]. These frictional interactions are complex primarily due to the high normal contact pressures, temperatures, and sliding speeds that vary throughout the tool/workpiece/chip interface. Therefore the COF cannot be assumed to be a constant value [2]. In addition, other factors such as surface asperities, the local deformation of the workpiece/chip, the presence of lubricants, tool-workpiece vibrations, and atmospheric properties further increase the complexity.

In drilling there are three main contact zones with different tribological conditions. These are the tool-chip, tool-workpiece, and tool-hole contacts, as discussed by Lorain et al.

[3]. The tool-chip and tool-workpiece contacts, in the secondary and tertiary deformation zones respectively, are open systems as the material is continuously refreshing. The tool-hole contact is where the minor cutting edge of the drill is in contact with the generated hole surface, this is a closed system as the tool rubs over a surface that has already been modified by the tool. The methods available to determine the COF fall into three categories, either by in-process cutting force measurement, conventional bench tribometers, or specialist high-speed tribometers designed to recreate the conditions of metal cutting [4].

The first category involves measuring the cutting forces during orthogonal cutting and using a shear zone based analytical model of metal cutting to determine an averaged apparent COF [5]. This method is idealised and limited as the analytical shear zone models usually assume a perfectly sharp cutting edge, and it does not allow the variation in the COF

along the tool/workpiece/chip interface to be determined. Several attempts have been made to address the latter issue by utilising either a split tool [6] or a partially restricted tool [7] to vary the tool-chip contact length and therefore capture the variation of frictional shear stresses and the COF along the rake face. The latter study demonstrates the presence of the stick-slip phenomena, contact pressure in the region of 1 – 2.25 GPa, and apparent COF values up to 2.6 in the slip region on the rake face of the tool. However, the limitations with this method are that the force contribution of the edge radius is calculated analytically, and the contact mechanics could be affected by the introduction of the slot on the rake face, which is not representative of real-world conditions.

Traditional pin-on-disc bench tribometers have been used to generate a sliding contact and determine the COF for machining simulations [8], however, the technique is not capable of recreating the conditions of metal cutting with respect to the high temperatures and contact pressures [9]. Additionally, the conventional setup only replicates a closed system where the pin repeatably travels over the same path. Therefore, the open system in the secondary and tertiary shear zones is not recreated. Modified setups have been designed to alleviate this issue where the pin follows a spiral path [10], however this requires very large discs for high cutting speeds.

Specialist open tribometers are an improvement on traditional pin-on-disc tests for machining applications. Open and closed system sliding contacts have been generated on the outer diameter of a bar using a lathe, with contact pressures and sliding speeds equivalent that observed in metal cutting [11]. However, the obtained temperatures were not reported, and the sliding contact occurs on a ground surface which may affect the results due to the presence of a surface oxidation layer that is not present at the tool/chip and tool/workpiece interfaces. To minimise the latter, experiments are reported whereby the pin immediately follows an orthogonal cutting pass on the end of a tube [12]; surface temperatures of 80 - 180°C were recorded before the pin passes over the surface at speeds of 1 – 3 m/s under a 1kN load, but temperature measurements during the contact were not captured.

It is reported in steels that the apparent COF reduces and the heat flux into the pin increases with an increased sliding speed [11]. Average contact pressures of between 1 - 3GPa [11] have been calculated using a geometry based method that relies on wear track width measurements.

To address some of the challenges in this context, this study reports a newly developed simplified high-speed tribometer for recreating the tribological conditions in drilling. The developed system is simplified so it does not require an additional pneumatic actuator to load the pin as reported in the literature. This study investigates how well the system replicates the tribology of drilling with respect to the local contact speeds, pressures, and temperatures, whilst studying the sub-surface modification which has been overlooked in previous literature.

2. Experimental Methodology

The material used in this study is the annealed C45U steel, with a ferritic-pearlitic microstructure and a chemical composition as reported in Table 1, in the form of bars with a diameter of 180 mm and a length of 135 mm. These had a uniform hardness of 199 HB. The bars were prepared using a turning operation, resulting in an average initial surface roughness of 1.25 μm Ra in the feed direction with a standard deviation of 0.022 μm.

Table 1. Chemical composition of C45U Annealed used in this study.

C	Si	Mn	P	S
0.48	0.280	0.740	0.01	0.03

2.1. Modified pin on bar setup

Fig. 1a shows the developed pin on bar setup and Fig. 1b shows the geometry of the TiNAl PVD coated tungsten carbide pins. The pins have two 0.5 mm diameter blind holes that extended to the centre line of the pins at distances of 1.5 mm and 4.5 mm from the point of contact. Transition joint TJC1-CASS-IM050U-150 0.5 mm diameter thermocouples were inserted into these holes and connected to a NI 9213 DAQ to measure the local pin temperatures and temperature gradient with a 75Hz sampling frequency. The surface roughness of a sample of 4 pins was measured prior to testing using an Alicona, the pins had an average surface roughness of 0.349 Ra with standard deviation of 0.08 Ra. The pins were mounted into a custom jig which was mounted to a Kistler 9213a dynamometer in a DMG Mori-Seiki NT4250 machine tool to measure the forces as demonstrated in Fig. 1a.
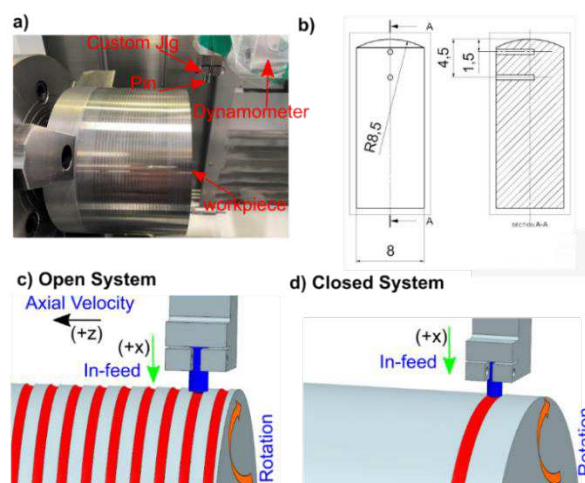

Fig. 1. (a) The experimental setup with (b) the drawing of the pin geometry (units in mm) and a demonstration of the (c) open and (d) closed tribometer.

The experiments were conducted by setting a constant indent depth (green arrow in Fig. 1c and Fig. 1d) into the rotating bar to generate the sliding contact. The open tribometer was created by using an axial feed rate of 2 mm/rev (black arrow in Fig. 1c) to avoid rubbing on the previous wear scar, generating a helical path on the bar. In contrast, the pin in the closed tribometer passed over a single path as shown in Fig. 1d in red. The open tribometer tests had a consistent steady-state engagement time of 8 seconds whilst the closed tribometer tests were engaged for a consistent 40 revolutions.

2.2. Experimental conditions

A range of testing conditions was selected for both the open and closed tribometers, based on an iterative preliminary study

using FEM in ABAQUS/Explicit, to ensure the pressures and sliding velocities were consistent with those in the tertiary and secondary shear zones during drilling. Instantaneous contact pressures from 1.6 - 2.3 GPa were predicted at indent depths from 5 - 150 μm, demonstrating that the instantaneous pressure is not significantly impacted by increasing indent depth due to the larger wear tracks produced.

It is worth noting that the dynamic instability and lack of consumables limited the maximum achievable speed and number of indent depths for the closed tribometer testing. Table 2 reports the designed experimental matrix, where green cells indicate open tribometer parameter sets, red cells indicate the closed tribometer parameter sets, and amber cells indicate parameter sets that both the open and closed tribometers were tested at.

Table 2. Experimental design matrix

In-feed (μm)	Sliding Speed (m/min)				
	10	**30**	**60**	**77.5**	**145**
50	Open/Closed	Closed	Closed	Open	Open
100	Open			Open	Open
150	Open/Closed	Closed	Closed	Open	Open

2.3. COF and heat flux calculation

The reactions forces were measured in the coordinate system shown in Fig. 1c and the tangential (out of plane direction in Fig. 1) and normal forces were calculated according to equations 1 and 2, respectively. This then allows the apparent COF to be determined using equation 3.

$$F_t = \sqrt{(F_y)^2 + (F_z)^2} \quad (1)$$

$$F_n = F_x \quad (2)$$

$$\mu_{app} = \frac{F_t}{F_n} \quad (3)$$

As there are two thermocouples in the pin the heat flux ($\dot{q}$) entering the pin can be calculated using Eqn.4 [13]. The thermal conductivity (k) used for the carbide pin is 110 W/mK, the area (A) is the cross-sectional area of the pin, and the length (L) is the 3 mm distance between the thermocouples.

$$\dot{q} = \frac{kA}{L}(T_1 - T_2) \quad (4)$$

It was assumed that the surface of the pin is perfectly insulated and that there are no convection losses. The latter is a reasonable assumption as no coolant was used, although the first assumption could potentially lead to an under prediction of the heat flux into the pin.

3. Results

Fig. 2a and Fig. 2c show the transient mechanical response of the open and closed tribometers, respectively. In the open tribometer (Fig.2a), the normal (red line) and tangential (green line) forces reached a steady-state rapidly, therefore so did the resultant COF (blue line). The slower closed tribometer tests, represented by the dashed lines in Fig. 2a, were run for longer

as these required more time to reach a steady-state, ensuring a consistent 8s of steady-state engagement was still achieved. The closed tribometer (Fig. 2c) takes much longer to reach a steady-state compared to the open tribometer (Fig. 2a), although this was eventually reached in all tests. As the number of cycles was kept constant in the closed tribometer tests, rather than the steady-state engagement time, this resulted in varied steady-state engagement times; approximately 2.5 s at 60 m/min and 100 s at 10 m/min.

Fig. 2b and Fig. 2d demonstrates the transient thermal response of the open and closed tribometers, respectively. The temperature measurements in both the open and closed tribometers did not reach a steady-state, however, the thermal heat flux energy entering the pin reached a steady-state rapidly. The heat flux is shown by the green lines and the local pin temperature measurements are shown by the red and blue lines in Fig. 2b and Fig. 2d for the open and closed tribometers respectively.
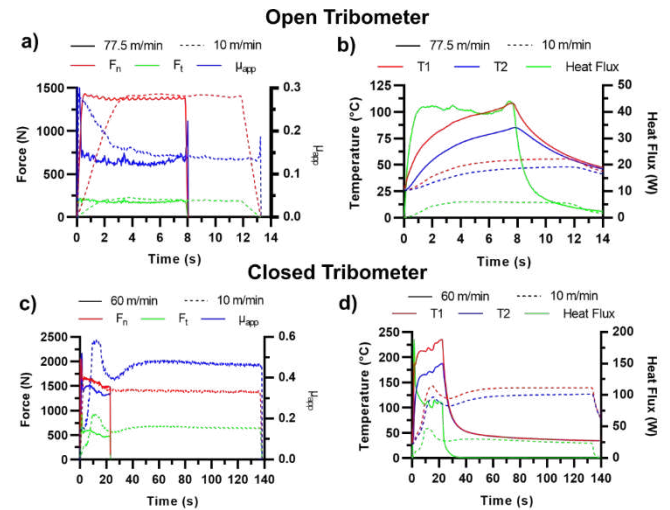

Fig. 2. The (a, c) mechanical and (b,d) thermal transient response of the open (a,b) and closed (c,d) tribometers at a 150μm indent. T1 and T2 are the thermocouple readings 1.5 and 4.5mm from the contact respectively.

The average apparent COF values in the steady-state engagement regions are plotted with respect to the normal load in Fig.4a and Fig.4b for the open and closed tribometers respectively. The data points at different surface speeds do not align with the same normal load, indicating that the normal load is a function of both in-feed depth and sliding speed.

In the open tribometer (Fig.3a) the apparent COF increases with the increased normal loads, while it is reduced with increased sliding speeds. However, there is a reduced change in the apparent COF with respect to the normal load above 1kN and with respect to the sliding speed above 77.5 m/min.

In the closed tribometer (Fig.3b), the apparent COF reduces as the normal load increases, which is the opposite trend to that observed in the open tribometer. However, the trends observed with respect to the sliding speed remain consistent with those observed previously. Due to the lower sliding speeds used and the reduced number of tests in the closed tribometer, there is no plateau in the apparent COF with respect to the sliding speed.

Comparing the open and closed tribometer tests at 10 m/min, the only tests directly comparable, this indicates that a much higher apparent COF value is reached in the closed

tribometer compared to the open tribometer; this is an increase of 0.4 at this sliding speed.
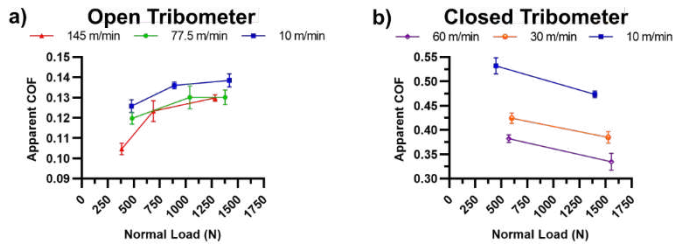

Fig.3. (a) OL and (b) CL apparent COF variation with normal load and sliding speed. Error bars show the standard deviation.

The average heat flux and maximum temperature reached (measured at T1) in the steady-state engagement region is shown in Fig. 4a and Fig. 4b for the open tribometer and Fig. 4c and Fig. 4d for the closed tribometer, respectively. Only the maximum absolute temperatures are plotted as a steady-state was not reached.

In both the open and closed tribometers, the trends are consistent, increasing the normal load and sliding speed results in increased heat flux and the maximum temperature recorded in the pin. Comparing the tests conducted at equal (10 m/min) sliding speed (blue lines in Fig. 4b and Fig. 4d for the open and closed tribometers, respectively), the maximum temperatures reached in the closed tribometer are approximately twice that measured in the open tribometer. This significant increase is likely due to the increased engagement time to reach 40 revolutions in the closed tribometer. Comparing the temperatures after the same engagement times in the 10 m/min tests, the closed tribometer still reached higher temperatures, albeit this increase is not as large as suggested by comparing Fig. 4b with Fig. 4d.
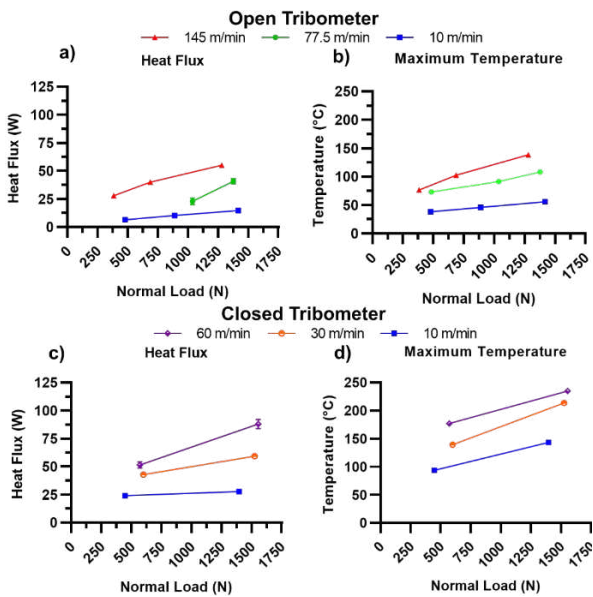

Fig. 4. (a,c) Average heat flux and (b,c) maximum temperature reached 1.5 mm from the surface in the open (a,b) and (c,d) closed tribometers.

3.1. Wear of the carbide pins

The wear on the pins used in the open tribometer testing was negligible (Fig. 5a), although this was more significant in the

closed tribometer testing (Fig. 5b). The width of the wear marks in the closed tribometer testing were measured, as indicated in Fig. 5b, these measurements are shown in Fig.6. This increases with both normal load and sliding speed, although there is very little difference at normal loads of around 500 N.
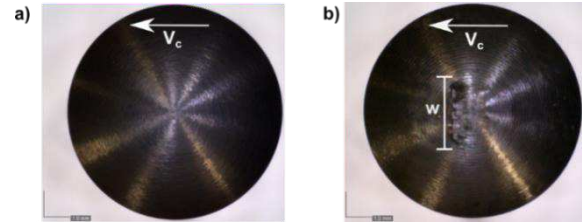

Fig. 5. Post-testing (a) Open (145 m/min and 150μm indent) and (b) closed tribometer pin (60 m/min and 150μm indent). Arrow shows travel direction.
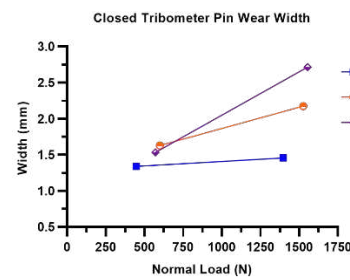

Fig.6. Closed tribometer testing pin wear mark widths at 10 m/min (blue line), 30 m/min (orange line), and 60 m/min (purple line).

3.2. Open loop contact area calculation

The produced wear track widths were measured using a Mutuyoto SJ-210 surface profile measurement tool. This method did not produce a detailed profile of the wear track, however, it was sufficient to measure the track width. In the open tribometer, the wear track widths (Fig. 8a) increase with the indent depth and reduce with increased sliding speed. In contrast, in the closed tribometer, the wear track widths increase with increased sliding speeds and produce larger wear tracks. Using equation 5 outlined by Zemzemi et al. [12], the averaged contact pressures for the open tribometer tests are calculated to be in the region of 1.4 – 1.8 GPa, as shown by the red lines in Fig. 7b. The closed tribometer pressure calculations are not shown in Fig. 7b due to the transient nature of the wear track geometry that was not captured. However, the calculated pressures using equation 5 are in the region of 0.48 – 0.7 GPa.
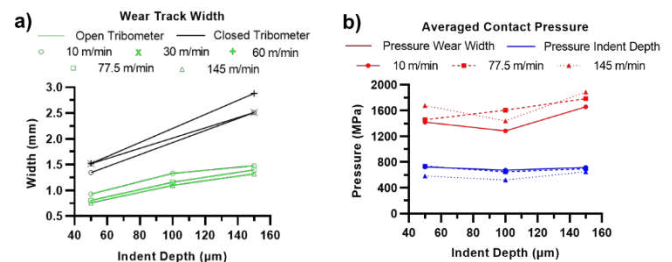

Fig. 7. (a) Measured wear track widths for the open (green lines) and closed (black lines) tribometers. (b) averaged contact pressure using the Zemzemi et al. [12] method (red lines) and indentation depth method (blue lines).

As the indent depth is already known, the contact area can be calculated without measuring the produced wear track using

equation 6. This is derived using a geometric relationship for the surface area of a half sphere sector (equation 7) and the empirical relationship between the in-feed depth (h) and contact area indent depth (h_c), as shown in Fig.8. The limitation of this method is that it requires the contact constant (k) to be known. This is commonly approximated as 2 [14], although a constant value likely does not represent the physics of the problem; further work to determine how this changes with the thermomechanical contact conditions is required.
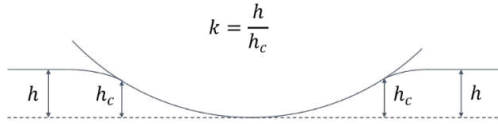
$$k = \frac{h}{h_c}$$

Fig.8. Indenter contact geometry, showing the contact constant k.

Fig. 7b shows that the applied method (blue lines) results in contact pressures approximately half of those obtained by the Zemzemi et al. [12] method (red lines). A contact constant (k) of 4 must be assumed to make the methods consistent. The difference in the predicted contact pressures using the two formulations is either related to an inaccurate contact constant (k), because the measured wear track widths (w_c) are not the instantaneous contact widths during the test due to the elastic relaxation when it is unloaded, or due to the deflection of the pin holder and the machine during loading. The measured wear track depth after testing at the 150 μm in-feed depth was only approximately 12 μm, indicating that it is likely primarily related to the deflection of the machine with a contribution from the wear track elastic recovery.

However, these methods only calculate an averaged contact pressure, the pressure of interest is the instantaneous contact pressure under the pin which can only be determined by inverse finite element modelling as outlined by Zemzemi et al. [12].

$$P \approx \frac{8F_n}{\pi W_c^2} \tag{5}$$

$$P = \frac{F_n}{A_c} \approx \frac{kF_n}{\pi Rh} \tag{6}$$

$$A_c = \pi Rh_c \tag{7}$$

3.3. Open loop wear scar surface integrity

Micrographs of the centre points of the wear tracks in the open tribometer tests are shown in Fig.9. This central point of the wear track is where the maximum instantaneous temperature and pressure is expected. Fig.9a and Fig.9b show the 50 μm in-feed tests and Fig.9c and Fig.9d depict the 150 μm in-feed tests at 10 m/min and 145 m/min, respectively. The thickness of the induced plastically deformed layer beneath the pin increases with increased sliding speed and in-feed depth. This layer does not have a consistent thickness throughout the contact surface, it has 'breaks' within the layer which appear to be heavily deformed ferrite grains within a region of deformed pearlite grains. Due to this inconsistency, it is difficult to quantify this, however at 50 μm in-feed the plastically deformed layer is approximately 1.261 and 3.166 μm at 10 and 145 m/min, respectively. These then increase to approximately 3.083 and 3.525 μm at a 150 μm in-feed, respectively.
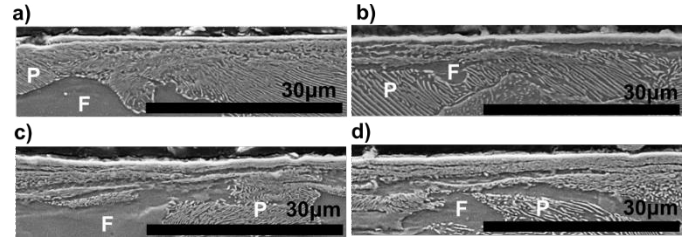

Fig.9. SEM images at the centre of the wear track with a 50μm in-feed at (a) 10 and (b) 145 m/min, and with a 150μm in-feed at (c) 10 and (d) 145 m/min.

4. Discussion

In the closed tribometer, the in-feed depth is fixed, therefore after the material is plastically deformed when the pin passes, the in-feed depth will be reduced in the subsequent passes. Although, as shown in the open tribometer, a large proportion of the deformation is elastically recovered so the in-feed depth should not be significantly impacted. This effect, along with the increased wear on the pins and the increasing plastic deformation of the workpiece likely contribute to the longer time required to reach a steady-state in the closed tribometer compared with the open tribometer.

In both the open and closed tribometers, the pin temperatures did not reach a steady-state although the heat flux reached a steady-state within approximately 1s. This phenomenon has also been previously reported [12] which is due to the low total engagement times.

Compared to the previous setups in the literature that apply a constant normal load using a pneumatic cylinder [11], it is not possible to maintain a constant normal load and vary the sliding speed. However, as demonstrated in this study, exact user control over the normal load is not required to characterise the COF with respect to the thermomechanical contact conditions. In the open tribometer, increasing the sliding speed with a constant in-feed depth generally reduces the normal load and increases the maximum temperature reached (shown in Fig. 4b) due to the increased thermal softening effect. In the closed tribometer, this trend is not observed, an increased sliding speed generally results in an increased normal load. This is likely because of the wear of the pins at higher sliding speeds and normal loads, as shown in Fig.6.

The trends observed in the closed tribometer with respect to the apparent COF have also been reported by other authors [11], [12]. In the closed tribometer, the reduction in the COF with increased normal load is likely due to the higher local temperatures compared with the open tribometer (Fig. 4b compared with Fig. 4d), causing increased thermal softening at higher loads. In the open tribometer, the range of the apparent COF throughout the experimental design space ($\sim 0.1 - 0.15$) is much lower than the range seen in the closed tribometer ($\sim 0.3 - 0.55$). This potentially suggests that the COF on the minor cutting edge of the drill is higher, and is more sensitive to the thermomechanical contact conditions, compared with the COF in the secondary and tertiary deformation zones. However, the increased absolute apparent COF values in the closed tribometer compared with the open tribometer are potentially also due to the larger contact areas (demonstrated in Fig. 7a), caused by the increased temperatures and plastic deformation.

The contact pressures in the OL system are in the region of 1.4 – 1.8 GPa using the Zemzemi equation, which is consistent with those experimentally measured in the secondary and tertiary shear zones during machining [7]. Although this equation only calculates an averaged contact pressure, this method has been shown to be consistent with the instantaneous maximum pressures predicted using FE modelling [11].

The measured temperatures in the pin were all below 150°C as the coating acts as a thermal barrier and the closest thermocouple in the pin was 1.5 mm from the point of contact. It is not possible to comment on whether the contact temperatures replicate that seen in drilling as the instantaneous contact temperatures are not known. The micrographs of the produced wear tracks indicate that potentially no phase transformation occurred, suggesting that the temperatures did not exceed the austenitisation temperature (723 ºC), which does not occur in orthogonal cutting at surface speeds below 200 m/min [15]. Therefore, in drilling operations at surface speeds below 145 m/min, this temperature should not be exceeded.

Due to the dynamic instability issues in the CL system, the maximum sliding speed achieved (60 m/min) does not replicate the sliding speeds on the minor cutting edge of the drill (around 80 – 145 m/min) using commercial cutting parameters. Further closed tribometer testing is required at higher sliding speeds and the instantaneous contact pressures and temperatures need to be calculated by inverse modelling the sliding contact conditions using FE modelling.

5. Conclusions

A new simplified high-speed pin on bar tribometer, that does not require a pneumatic actuator to control the applied normal load, has been developed and used to study both open and closed systems. The apparent COF values in the closed tribometer are much higher than those observed in the open tribometer. This suggests that the COF on the minor cutting edge of the drill is higher than in the secondary and tertiary shear zones. In the open tribometer, the apparent COF increases with increased normal load and decreases with increased sliding speed. However, in the closed tribometer, although the same trend with respect to sliding speed is observed, the apparent COF decreases with an increased normal load.

The averaged contact pressures were calculated using a geometric method based on the wear track measurements, indicating that the contact pressures are in the region of 1.4 – 1.8 GPa, which is consistent with those in machining. The sliding speeds used in the open tribometer testing were within the range expected in drilling, however, the speeds in the closed tribometer were below those expected at the minor cutting edge of the drill because of the dynamic instability issues. As the contact temperatures were measured in the pin, the instantaneous contact temperatures are not known. The micrographs of the wear tracks indicate that phase transformation did not occur, suggesting that the temperatures did not exceed 723 °C, which is consistent with drilling at commercially recommended speeds. The plastically deformed layer beneath the pin consisted of heavily deformed pearlite and ferrite grains, which increase in thickness as the normal load and sliding speed is increased.

Further FE modelling is required to determine the instantaneous pressures and temperatures beneath the pin. In addition, higher speed closed tribometer testing with analysis of the wear track surface integrity is required.

References

[1] T. Özel, "The influence of friction models on finite element simulations of machining," *Int. J. Mach. Tools Manuf.*, vol. 46, no. 5, pp. 518–530, 2006.

[2] J. Priest, H. Ghadbeigi, S. Ayvar-Soberanis, and A. Liljerehn, "Effects of coefficient of friction coupled with a deformation dependent friction model in cutting simulations," *Procedia CIRP*, vol. 102, pp. 429–434, 2021.

[3] R. Lorain, L. Olivier, A. Poggi, F. Valiorgue, and J. Rech, "Identification of friction coefficients when drilling titanium TiAl6V4," *Procedia CIRP*, vol. 82, pp. 119–123, 2019.

[4] W. Grzesik and J. Rech, "Development of tribo-testers for predicting metal cutting friction," *J. Mach. Eng.*, vol. 19, no. 1, pp. 62–70, 2019.

[5] W. Grzesik and P. Nieslony, "Prediction of friction and heat flow in machining incorporating thermophysical properties of the coating-chip interface," *Wear*, vol. 256, no. 1–2, pp. 108–117, 2004.

[6] S. Kato, K. Yamaguchi, and M. Yamada, "Stress Distribution at the Interface Between Tool and Chip in Machining," *J. Eng. Ind.*, vol. 94, no. 2, p. 683, 1972.

[7] G. Ortiz-de-Zarate, A. Madariaga, P. J. Arrazola, and T. H. C. Childs, "A novel methodology to characterize tool-chip contact in metal cutting using partially restricted contact length tools," *CIRP Ann.*, vol. 70, no. 1, pp. 61–64, 2021.

[8] V. Schulze, J. Michna, J. Schneider, and P. Gumbsch, "Modelling of cutting induced surface phase transformations considering friction effects," *Procedia Eng.*, vol. 19, pp. 331–336, 2011.

[9] W. Grzesik, Z. Zalisz, and P. Nieslony, "Friction and wear testing of multilayer coatings on carbide substrates for dry machining applications," *Surf. Coatings Technol.*, vol. 155, no. 1, pp. 37–45, 2002.

[10] L. Meier, N. Schaal, and K. Wegener, "In-process Measurement of the Coefficient of Friction on Titanium," *Procedia CIRP*, vol. 58, pp. 163–168, 2017.

[11] F. Zemzemi, J. Rech, W. Ben Salem, A. Dogui, and P. Kapsa, "Identification of a friction model at tool/chip/workpiece interfaces in dry machining of AISI4142 treated steels," *J. Mater. Process. Technol.*, vol. 209, no. 8, pp. 3978–3990, 2009.

[12] F. Zemzemi, W. Bensalem, J. Rech, A. Dogui, and P. Kapsa, "New tribometer designed for the characterisation of the friction properties at the tool/chip/workpiece interfaces in machining," *Lubr. Sci.*, pp. 11–25, 2008.

[13] M. Çengel, Yunus A; Boles, Michael A; Kanoglu, *Thermodynamics : An Engineering Approach*, 9th ed. Boston: McGraw-Hill Higher Education, 2008.

[14] S. V. Kontomaris and A. Malamou, "Hertz model or Oliver & Pharr analysis? Tutorial regarding AFM nanoindentation experiments on biological samples," *Mater. Res. Express*, vol. 7, no. 3, 2020.

[15] S. Han, S. N. Melkote, M. S. Haluska, and T. R. Watkins, "White layer formation due to phase transformation in orthogonal machining of AISI 1045 annealed steel," *Mater. Sci. Eng. A*, 2008.